crystals

MDPI

Article

Synthesis, Structure and Physical Properties of (trans-TTF-py_2)$_{1.5}$(PF_6)·EtOH: A Molecular Conductor with Weak CH···N Hydrogen Bondings

Shohei Koyama [1], Morio Kawai [1], Shinya Takaishi [1], Masahiro Yamashita [1,2], Norihisa Hoshino [3], Tomoyuki Akutagawa [3], Manabu Kanno [1] and Hiroaki Iguchi [1,*]

1 Department of Chemistry, Graduate School of Science, Tohoku University, 6-3 Aramaki-Aza-Aoba, Aoba-ku, Sendai 980-8578, Japan; shohei.koyama.t3@dc.tohoku.ac.jp (S.K.); morio118ts@gmail.com (M.K.); shinya.takaishi.d8@tohoku.ac.jp (S.T.); yamasita.m@gmail.com (M.Y.); manabu.kanno.d2@tohoku.ac.jp (M.K.)

2 School of Materials Science and Engineering, Nankai University, Tianjin 300350, China

3 Institute of Multidisciplinary Research for Advanced Materials, Tohoku University, 2-1-1 Katahira, Aoba-ku, Sendai 980-8577, Japan; norihisa.hoshino.b5@tohoku.ac.jp (N.H.); akutagawa@tohoku.ac.jp (T.A.)

* Correspondence: h-iguchi@tohoku.ac.jp

Received: 31 October 2020; Accepted: 24 November 2020; Published: 26 November 2020

Abstract: The studies of crystal structures with hydrogen bonds have been actively pursued because of their moderate stabilization energy for constructing unique structures. In this study, we synthesized a molecular conductor based on 2,6-bis(4-pyridyl)-1,4,5,8-tetrathiafulvalene (trans-TTF-py_2). Two pyridyl groups were introduced into the TTF skeleton toward the structural exploration in TTF-based molecular conductors involved by hydrogen bonds. In the obtained molecular conductor, (trans-TTF-py_2)$_{1.5}$(PF_6)·EtOH, short contacts between the pyridyl group and the hydrogen atom of the TTF skeleton were observed, indicating that hydrogen bonding interactions were introduced in the crystal structure. Spectroscopic measurements and conductivity measurement revealed semiconducting behavior derived from π-stacked trans-TTF-py_2 radical in the crystal structure. Finally, these results are discussed with the quantified hydrogen bonding stabilization energy, and the band calculation of the crystal obtained from density functional theory calculation.

Keywords: tetrathiafulvalene; molecular conductor; hydrogen bonding

1. Introduction

Since the first metallic molecular conductor, TTF-TCNQ was reported [1], many researchers have been eagerly exploring TTF-based charge-transfer complexes [2,3], and exotic physical properties have been reported in well-designed molecular crystals in recent years [4,5]. In the progress of molecular conductors, modulating crystal structures has been one of the biggest challenges because the physical properties of molecular conductors heavily depend on their structures. Up to now, there have been several attempts to manipulate crystal structures by introducing supramolecular interactions into the TTF skeleton, such as intermolecular hydrogen bond [6–12] and halogen bond [6,13–16]. Among them, utilizing the hydrogen bond has been gathering attention because of its ability to form various unique structures owing to the moderate bond-dissociation energy (~40 kcal/mol) [17]. Although developments of TTF-based molecular crystals with hydroxy, amide, and cyano groups have been reported so far [6–12], TTF-based molecular conductors with pyridyl groups have been scarcely reported [18,19]. Furthermore, the pyridyl group in the TTF skeleton has often been used for metal coordination [20,21] but not for hydrogen bonding. The hydrogen bonding via pyridyl groups has many advantages in the arrangement of crystal structures because of its well-directed interaction derived from the rigid

structure of the pyridyl group. In addition, the pyridyl group is easy to be introduced into π-conjugated molecular backbones by applying a hetero coupling reaction [22]. To investigate a novel crystal structure of TTF-based molecular conductors, we chose 2,6-bis(4-pyridyl)-1,4,5,8-tetrathiafulvalene (trans-TTF-py_2) as a starting material. This molecule has two pyridyl groups on the TTF skeleton (Scheme 1), and a unique structure based on a hydrogen bonding via the pyridyl groups can be expected. Although TTF-py_2 has been reported as a neutral molecular crystal [23] and as a ligand in coordination polymers [24–28], there is no report of trans-TTF-py_2-based conductive crystal. Even in trans-bis-substituted TTF molecules, the crystal structure of the molecular conductor was reported in only one paper to the best of our knowledge [29]. In our paper, a molecular conductor, (trans-TTF-py_2)$_{1.5}$(PF_6)·EtOH (**TTF-py_2_PF_6**), was prepared through electrochemical crystallization. Single crystal X-ray diffraction (SXRD) revealed a one-dimensional π-stacking structure of oxidized trans-TTF-py_2, where the nitrogen atoms of the pyridyl groups have short contacts with hydrogen atoms of the adjacent TTF-py_2 molecules, suggesting the existence of significant hydrogen bondings. Spectroscopic analyses and the measurement of electrical conductivity of **TTF-py_2_PF_6** were carried out. Its band structure and the stabilization energy of hydrogen bondings calculated by density functional theory (DFT) are also discussed.

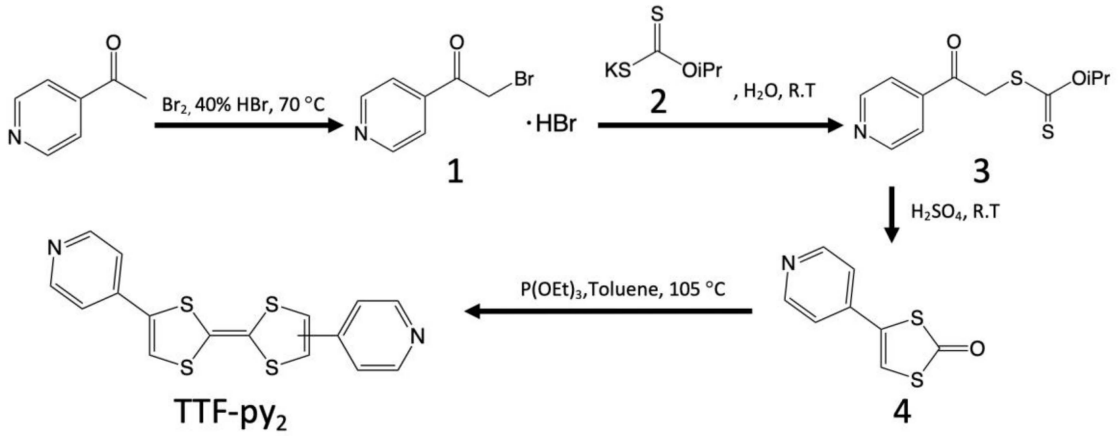

Scheme 1. Synthesis of TTF-py_2.

2. Materials and Methods

2.1. Methods

All solvents and reagents used in the syntheses were obtained from commercial sources without further purification. IR spectrum was recorded as KBr pellets on a FT/IR-4200 spectrometer of JASCO, Tokyo, Japan at room temperature (RT). UV-Vis-NIR absorption spectrum was measured as KBr pellets on a V-670 spectrophotometer of JASCO, Tokyo, Japan at RT. Both spectra were connected to represent the solid-state absorption spectrum in a wide range (Figure 2b). The ESR spectra were acquired by using a JES-FA100 of JEOL, Tokyo, Japan. Microscopic Raman Spectrum was measured by using a LabRAM HR-800 of HORIBA, Kyoto, Japan at RT.

^{1}H NMR measurements were performed on Bruker AV500 of Bruker Japan, Kanagawa, Japan at RT. The temperature dependence of the electrical conductivity was measured in a liquid He cryostat of a Quantum Design Physical Property Measuring System (PPMS) MODEL 6000 of Quantum Design Japan, Tokyo, Japan by using the two-probe method in direct current (DC) mode with Keithley sourcemeter model 2611 of Tektronix, Beaverton, Oregon, United States. The cooling rate was 2 K/min. The electrical leads (15 μmφ gold wires) were attached to a single crystal with carbon paste (Dotite XC-12 in diethyl succinate).

2.1.1. Single X-ray Diffraction

The diffraction data for **TTF-py$_2$_PF$_6$** were collected on a XtaLAB AFC10 diffractometer with a HyPix-6000HE hybrid pixel array detector, graphite monochromated Mo Kα radiation (λ = 0.7107 Å) and a cryogenic equipment GN-2D/S of Rigaku, Tokyo, Japan. The crystal structure was solved using direct methods (SHELXT) followed by Fourier synthesis. Structure refinement was performed using full matrix least-squares procedures with SHELXL [30,31] on *F* [2], where *F* is the crystal structure factor, in the Olex2 software. [32]

2.1.2. Computational Methods

DFT calculations were performed using the gaussian 16 package [33] for estimation of hydrogen bonding with the counterpoise method [34]. The B3LYP functional [35–37] and the cc-pVTZ basis sets [38] were used for the calculation of hydrogen bonding, because the B3LYP functional has been validated in previous studies for the calculation of hydrogen bonds in several models such as clathrate, radical, and cation-anion systems [39–42]. The atomic coordination of trans-TTF-py$_2$ ligands was extracted from the cif files of **TTF-py$_2$_PF$_6$** reported herein and used for the calculation without any optimizations. The molecular orbital energies were presented against the vacuum level standard.

Amsterdam Modeling Suite (AMS) packages were applied for the calculations of charge transfer integrals [43,44] and band structure [45] with tight-binding approximation. Charge transfer integrals between adjacent trans-TTF-py$_2$ molecules and band structure of **TTF-py$_2$_PF$_6$** were investigated by the B3LYP/TZP method, and third-order density-functional-based tight binding (DFTB3) model, respectively, without structural optimization.

2.2. Syntheses

TTF-py$_2$ was synthesized by following already described procedures [46] (Scheme 1) with a little modification (e.g., reaction temperature and the solvent used for washing in the synthesis of **1**, reaction temperature and the addition of the extraction process in the synthesis of **2,** reaction temperature in the reaction in the synthesis of **3**, and recrystallization process in the synthesis of **4**).

2.2.1. Synthesis of 4-(2-bromoacetyl)pyridine Hydrobromide (**1**)

Bromine (20.00 g, 0.13 mol) was added dropwise to 4-acetylpyridine (15.36 g, 0.13 mol) dissolved in 40 mL of HBr aq.(47–49% wt.) at 70 °C. Transparent crystalline solid was immediately precipitated in the solution after the addition of bromine. The precipitate was filtered, washed with acetonitrile, and dried in a desiccator to obtain 4-(2-bromoacetyl)pyridine hydrobromide. Yield: 74.8% ^{1}H NMR (500 MHz, D_2O, 298 K, ppm) δ 8.78 (d, 2H), 8.19 (d, 2H), 3.72 (s, 2H).

2.2.2. Synthesis of Potassium Isopropylxanthate (**2**)

Potassium hydroxide (14.03 g, 0.25 mol) were dissolved in 100 mL isopropanol at 80 °C and then cooled to 40 °C. Pale pinkish suspension was obtained after carbon disulfide (19.04 g, 0.25 mol) were slowly added dropwise to the solution. The precipitate was filtered and extracted with acetone to obtain a bright yellow crystalline solid. Yield: 76.3%. ^{1}H NMR (500 MHz, $CDCl_3$, 298 K, ppm) δ 5.33 (sep, 1H), 1.35 (d, 6H).

2.2.3. Synthesis of O-(1-methylethyl)S-[2-oxo-2-(4-pyridinyl)ethyl]carbonodithioate (**3**)

1 (7.02 g, 25 mmol) dissolved in 75 mL H_2O and **2** (1.30 g, 38 mmol) dissolved in 50 mL H_2O were mixed with stirring. Formed transparent crystals were filtered, washed with H_2O, and dried in a desiccator overnight to give **3**. Yield: 77.8% ^{1}H NMR (500 MHz, $CDCl_3$, 298 K, ppm) δ 8.86 (d, 2H), 7.80 (d, 2H), 5.70(sep, 1H), 4.59 (s, 2H), 1.38 (d, 6H).

2.2.4. Synthesis of 4-(4-pyridyl)-1,3-dithiol-2-one (**4**)

3 (4.9 g,19 mmol) was dissolved in 7.5 mL conc. H_2SO_4, and the resulting black solution was heated to 50 °C for 30 min. The solution was poured into 200 mL of H_2O, neutralized by $NaHCO_3$, and extracted with dichloromethane. The solvent was dried with $MgSO_4$ and evaporated to obtain a brown solid. This solid was recrystallized with EtOH to get a brown crystalline solid. ^{1}H NMR (500 MHz, $CDCl_3$, 298 K, ppm) δ 8.70 (d, 2H), 7.33 (d, 2H), 7.18 (s, 1H).

2.2.5. Synthesis of TTF-py_2 (the Mixture of cis and trans Isomers)

4 (2.0 g,10 mmol) was suspended in 10 mL dehydrated toluene and 10 mL dehydrated $P(OEt)_3$ under N_2 atmosphere. This suspension was heated to 105 °C for 4 h. Red precipitate was filtered, washed with MeOH, and recrystallized with nitromethane to acquire red crystalline solid. ^{1}H NMR (500 MHz, $CDCl_3$, 298 K, ppm) δ 8.63 (2H), 7.77 (1H), 7.47 (2H). Since two structural isomers are produced in the synthesis of TTF-py_2 (cis-TTF-py_2 and trans-TTF-py_2), we had difficulty in assigning the correct coupling from this NMR spectrum. Anal. Calcd for $C_{16}H_{10}N_2S_4$: C, 53.60; H, 2.81; N, 7.81; S, 35.77. Found: C, 53.21; H, 2.85; N, 7.99; S, 35.44.

2.2.6. Synthesis of (trans-TTF-py_2)$_{1.5}$(PF_6)·EtOH (TTF-py_2_PF_6)

TTF-py_2, which is the mixture of cis and trans isomers (10 mg, 28 μmol), and $TBAPF_6$ (40 mg, 104 μmol) were dissolved in 10 mL of $CHCl_3$/EtOH (7:3, *v*/*v*) solution. A constant current of 2.5 μA was applied to the solution. After a week, black needle crystals were isolated from the anode, and subsequently washed by $CHCl_3$ and EtOH followed by drying in air. Anal. Calcd for $C_{26}H_{21}F_6N_3OPS_6$: C, 42.85; H, 2.90; N, 5.77; S, 26.40; Cl, 0.00. Found: C, 42.32; H, 2.74; N, 5.85; S, 26.46; Cl, 0.06.

3. Results

3.1. Crystal Structure

The trans-TTF-py_2-based molecular conductor, **TTF-py_2_PF_6**, was obtained through electrochemical crystallization in a $CHCl_3$/EtOH (7:3, *v*/*v*) solution dissolving TTF-py_2 and $TBAPF_6$ [47]. The similar conditions with $TBAClO_4$, $TBABF_4$, or TBAX (X = Cl and Br) did not give any crystals. Single-crystal X-ray structure analysis shows two hexafluorophosphates for every three trans-TTF-py_2 molecules, indicating that the average charge of trans-TTF-py_2 is +0.66 (Figure 1). The cis isomer was not incorporated into the crystal. Two crystallographically independent trans-TTF-py_2 (**A** and **B**) molecules exist in the crystal structure (Figure 1a), repeating the **A**–**B**–**B** order to form a one-dimensional columnar structure by π–π stacking. The closest intermolecular S···S distances between adjacent trans-TTF-py_2 molecules along the π-stack axis are summarized in Table 1. This table indicates that the S···S distances between **A**–**B** are shorter than the sum of van der Waals radius of the sulfur atoms (3.60 Å) [48], whereas those between **B**–**B** are longer than that value. In fact, the side view of the π-stacking structure (Figure 1c) clearly shows that the shift of π-stacking between **B** and **B** is larger than that between **A** and **B**. Focusing on the environment of π-stack columnar structures (Figure 1d,e), one π-stack column is surrounded by four other columns. Figure 1d,e highlight the interactions of **A** and **B** with neighboring molecules, respectively. It is noteworthy that there are short contacts between the nitrogen atoms of the pyridyl groups and the hydrogen atoms of TTF cores, emphasized with orange broken lines in Figure 1d and e. **A** is surrounded by four **B** molecules and has short contacts with two of them. **B**, on the other hand, is surrounded by two each of **A** and **B**, and it interacts with all but one **A**. The intermolecular N···H distances are 2.365 Å (between **A** and **B**) and 2.626 Å (between **B** and **B**), which are shorter than the sum of the van der Waals radii of hydrogen and nitrogen atoms [48], suggesting the construction of C–H···N hydrogen bondings. To obtain a deeper insight into the hydrogen bondings connecting trans-TTF-py_2 molecules, a DFT calculation was applied for estimating stabilization energies of the hydrogen bondings between **A** and **B** and **B** and **B** depicted in Figure 1d,e. The calculation indicated that the stabilization energies are –0.74 kcal/mol for the hydrogen bonding

between **A** and **B** and –1.72 kcal/mol for that between **B** and **B**. Hence, the sum of the stabilization energies of the hydrogen bondings around **A** is –1.48 kcal/mol (= 2 × (–0.74) kcal/mol) and that around **B** is –4.18 kcal/mol (= 2 × (–1.72) –0.74 kcal/mol). Calculated effective transfer integrals (V_{eff}) between neighboring trans-TTF-py_2 molecules along the columnar structure are V_{eff}(A–B) = 390.8 meV for **A**–**B** and V_{eff}(B–B) = 222.9 meV for **B**–**B** (Figure 1c), reflecting the difference in the stacking feature. On the other hand, V_{eff} of trans-TTF-py_2 molecules between adjacent columns are less than 10 meV in all combinations. This much difference of V_{eff} obviously demonstrates the character of one-dimensional electron conductor in **TTF-py$_2$_PF$_6$**.

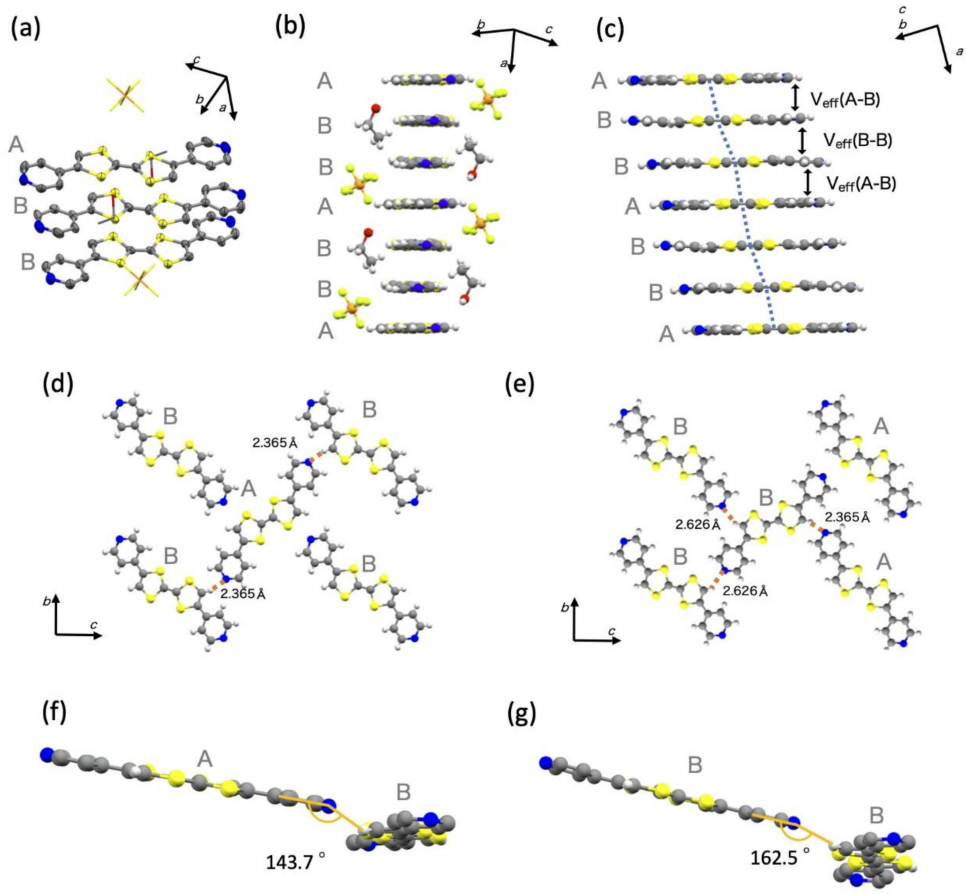

Figure 1. Crystal structure of **TTF-py$_2$_PF$_6$**. (**a**) Thermal ellipsoid plot of **TTF-py$_2$_PF$_6$**. Counteranion (PF_6^-) and crystal solvent (EtOH) were pictured in capped sticks, and hydrogen atoms are omitted for clarity. (**b**,**c**) π-stacked TTF-py_2 columns viewed from different sides. Blue broken lines are written to represent the shift of π-stacks. Counteranion and crystal solvent were omitted for clarity in (**c**). (**d**,**e**) Perspective views of **TTF-py$_2$_PF$_6$** along the *a* axis with placing **A** or **B** at the center, respectively. Short contacts with neighboring columns are represented as broken orange lines. (**f**,**g**) View of the angle of the hydrogen bonding site between **A** and **B** (**f**) and **B** and **B** (**g**). Hydrogen atoms of pyridyl groups were omitted for clarity. Yellow, S; Orange, P; Light green, F; Red, O; Blue, N; Gray, C; White, H.

Table 1. The distances between the nearest sulfur atoms along the π-stack axis.

	A–B	**B–B**
Intracolumnar S···S distance/Å	3.584 3.481 3.493 3.408	3.701 3.666

3.2. Electronic States and Conductivity of TTF-py_2_PF_6

To understand the electronic state of **TTF-py_2_PF_6**, microscopic Raman spectrum, solid-state absorption spectrum, and ESR spectrum of **TTF-py_2_PF_6** were recorded and shown in Figure 2. Microscopic Raman spectrum of **TTF-py_2_PF_6** shows a strong peak around 1450 cm^{-1} and weak peaks around 1420 and 1520 cm^{-1}. It is well known that there is a correlation between the valence of the TTF molecule and Raman frequency [49], and the valence corresponding to 1450 cm^{-1} is found to be about +0.6 based on previous studies [49]. This value is in approximate agreement with the valence obtained from the formula, +0.66. The absorption spectrum consists of major absorption bands above 1.7 eV, a broad band around 0.4 eV, and a minor band around 1.5 eV (Figure 2b). Each band was assigned by following previous reports [50–52]. Major bands above 1.7 eV correspond to the mixture of the π–π* transition for the radical monomer trans-TTF-$py_2^{\bullet+}$ and radical dimer (trans-TTF-$py_2^{\bullet+}$)$_2$. A broad band around 0.4 eV and a minor band around 1.5 eV are characteristics of intermolecular charge transfer from trans-TTF-$py_2^{\bullet+}$ to trans-TTF-py_2^0 (forming trans-TTF-py_2^0 and trans-TTF-$py_2^{\bullet+}$) and from trans-TTF-$py_2^{\bullet+}$ to trans-TTF-$py_2^{\bullet+}$ (forming trans-TTF-py_2^0 and trans-TTF-py_2^{2+}), respectively [53]. The existence of trans-TTF-$py_2^{\bullet+}$ was also supported by the results of the ESR spectrum (Figure 2c), which shows a singlet peak with g = 2.003 derived from a TTF radical.

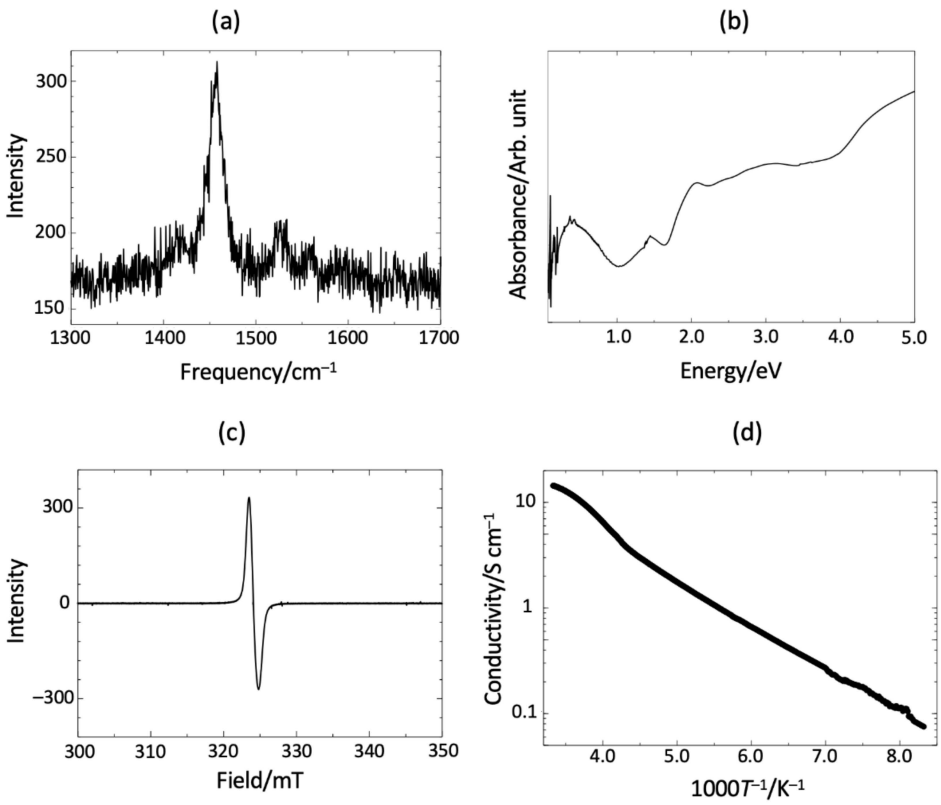

Figure 2. (**a**) Raman spectrum, (**b**) solid-state absorption spectrum from IR to UV energy region, (**c**) ESR spectrum, and (**d**) temperature-dependent electrical conductivity of **TTF-py_2_PF_6**.

A single crystal direct-current conductivity (= σ) of **TTF-py_2_PF_6** along the π-stack direction is shown in Figure 2d. The electrical conductivity of **TTF-py_2_PF_6** is 12 S cm^{-1} at RT, and the decreases with cooling temperature, suggesting semiconducting behavior. The slope of the Arrhenius plot is constant with $1000T^{-1}$ above 4.5 K^{-1}. From the fitting of the Arrhenius plot above 4.5 K^{-1} with an Arrhenius dependence of $\sigma = \sigma_0 \exp[-(E_g/2kT)]$ where σ_0 is a constant, E_g is the bandgap and k is Boltzmann constant [54], it shows that the E_g of the carriers is estimated to be 162 meV.

4. Discussion

The structural study shows short contacts by the hydrogen bondings, and the DFT calculation with the counterpoise correction shows the significant stabilization energy. It is noteworthy that although the distance of the hydrogen bonding between **A** and **B** (2.365 Å) is shorter than that between **B** and **B** (2.626 Å), the stabilization energy of the hydrogen bonding between **A** and **B** (= –0.74 kcal/mol) is less than that between **B** and **B** (= –1.72 kcal/mol). This tendency did not change even when the exchange correlation functional was changed from B3LYP to B3PW91 or PBEPBE in the DFT calculations. The nature of the hydrogen bond is complicated by the fact that the hydrogen bond has multiple parameters such as angles, distances and chemical species (elements of hydrogen donor and acceptor atoms). [17,55]. In the present case, the N···H distance seems to be less important to determine the energy of the hydrogen bond. As shown in Figure 1f,g, the angles between the axis of the pyridyl groups and the hydrogen atoms of the TTF core (∠C(position 4)···N···H) are 143.7° for **A** and **B** and 162.5° for **B** and **B**. Because the latter angle is closer to 180°, where the lone pair of nitrogen atom is headed to the hydrogen atom, the hydrogen bonding between **B** and **B** is stronger than that between **A** and **B**. Wood et al. examined the distance- and the angle-dependence of hydrogen bondings with pyridine in terms of computational chemistry [55]. In the paper, the structural dependence of the stabilization energy varies with chemical species, and the dependence of the energy on the interatomic distance is found to be relatively weak for the weak hydrogen bondings such as those with benzene. Even in this system, the hydrogen bondings are also weak C-H···N bonds, thus the dependence of the energy on the N···H distance is small, and the change of the angle is more likely to be involved in the stabilization energy.

The temperature-dependent electrical conductivity of **TTF-py$_2$_PF$_6$** shows semiconducting behavior along the *a* axis. Effective charge transfer integrals of adjacent TTF-py$_2$ clarify the nature of one-dimensional electron conductivity along the *a* axis, which is also denoted from the band structure. Given the difference of the effective charge transfer integral between **A** and **B** (V_{eff} = 390.8 meV), and **B** and **B** (V_{eff} = 220.9 meV), the semiconducting behavior of **TTF-py$_2$_PF$_6$** is probably due to the localization of carriers in the columnar structure. In fact, band calculation by using tight-binding approximation without structural optimization (Figure 3) shows an inherent bandgap, E_g = 140 meV, and hence a significant localization of carrier can be assumed from the crystal structure. The Calculated bandgap is almost consistent with the bandgap acquired from temperature-dependent conductivity (E_g = 162 meV). The carriers in the dominant part of the electron conduction were located where the path of the band structure is along a^* axis, the direction of π–π stacking of TTF-py$_2$. Hence, not only the effective charge transfer integrals but also the band structure show the one-dimensional conducting character of **TTF-py$_2$_PF$_6$**.

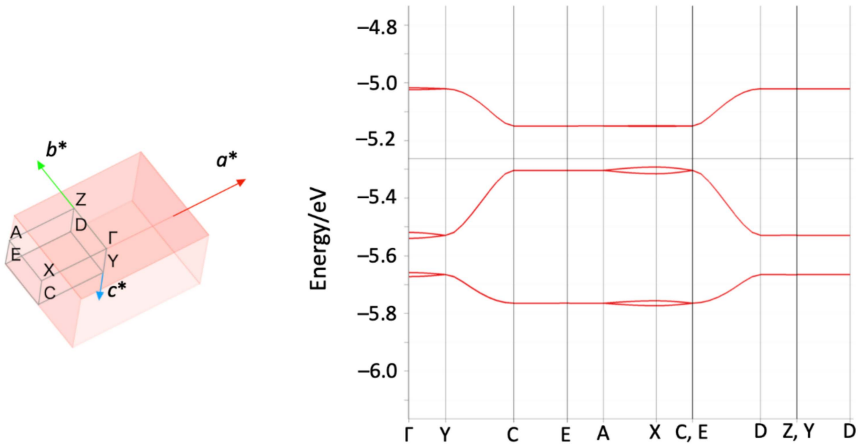

Figure 3. Brillouin zone of TTF-py2_PF6 (**left**) showing the path corresponding to the band structure of TTF-py2_PF6 (**right**).

5. Conclusions

In this paper, we discussed the crystal structure and the physical properties of the molecular conductor **TTF-py$_2$_PF$_6$**. It is the first molecular conductor containing trans-TTF-py$_2$ molecules and is the second one with trans-bis-substituted TTF molecules, to the best of our knowledge. Although **TTF-py$_2$_PF$_6$** has one dimensional electron transport properties, which is typical in molecular conductors, the hydrogen bondings between the pyridyl groups and the hydrogen atoms of the TTF skeleton were successfully introduced in the crystal structure. We believe that this result provides a potential for further structural explorations and physical properties of TTF-based molecular conductors with a substitution group with hydrogen bondings such as pyridyl and other moieties. Additionally, TTF-py$_2$ is a promising ligand for constructing both conductive π-stacked arrays and coordination networks in a crystal, such as porous molecular conductors [56,57] and conductive π-stacked metal-organic frameworks [58–61].

CCDC-2040487 contains the supplementary crystallographic data for this paper. Crystal structure information is available online at the Cambridge Crystallographic Data Centre (CCDC) database via www.ccdc.cam.ac.uk/data_request/cif.

Author Contributions: Conceptualization, S.K. and H.I.; methodology, S.K.; software, S.K., H.I.; validation, H.I., S.T. and M.K. (Manabu Kanno); formal analysis, S.K.; investigation, S.K., M.K. (Morio Kawai); resources, H.I., S.T., N.H., T.A.; data curation, S.K.; writing—original draft preparation, S.K.; writing—review and editing, H.I., S.T. and M.Y.; visualization, S.K.; supervision, H.I., and M.Y.; project administration, H.I. and S.T.; funding acquisition, S.K., H.I., and S.T. All authors have read and agreed to the published version of the manuscript.

Funding: This work was partly supported by JSPS KAKENHI Grant Numbers JP18H04498 (H.I.) for "Soft Crystals", JP18K14233 (H.I.), JP19H05631 (H.I., S.T. and M.Y.) and JP20J22404 (S.K.), by the Toyota Riken Scholar Program (H.I.) and by the Kato Foundation for Promotion of Science KJ-2916 (H.I.).

Acknowledgments: Authors acknowledge the Research and Analytical Center for Giant Molecules, Graduate School of Science, Tohoku University, for the measurement of elemental analysis and common equipment unit of Advanced Institute of Material Research, Tohoku University, for the measurement of microscopic Raman spectra.

Conflicts of Interest: The authors declare no conflict of interest.

References

1. Ferraris, J.; Cowan, D.O.; Walatka, V.; Perlstein, J.H. Electron transfer in a new highly conducting donor-acceptor complex. *J. Am. Chem. Soc.* **1973**, *95*, 948–949. [CrossRef]
2. Frère, P.; Skabara, P.J. Salts of extended tetrathiafulvalene analogues: Relationships between molecular structure, electrochemical properties and solid state organisation. *Chem. Soc. Rev.* **2005**, *34*, 69–98. [CrossRef] [PubMed]
3. Otsubo, T.; Takimiya, K. Recent Synthetic Advances of Tetrathiafulvalene-Based Organic Conductors. *Bull. Chem. Soc. Jpn.* **2004**, *77*, 43–58. [CrossRef]
4. Yamochi, H.; Koshihara, S. Organic metal (EDO-TTF)2PF6 with multi-instability. *Sci. Technol. Adv. Mater.* **2009**, *10*, 024305. [CrossRef] [PubMed]
5. Ueda, A. Development of Novel Functional Organic Crystals by Utilizing Proton- and π-Electron-Donating/Accepting Abilities. *Bull. Chem. Soc. Jpn.* **2017**, *90*, 1181–1188. [CrossRef]
6. Fourmigué, M.; Batail, P. Activation of Hydrogen- and Halogen-Bonding Interactions in Tetrathiafulvalene-Based Crystalline Molecular Conductors. *Chem. Rev.* **2004**, *104*, 5379–5418. [CrossRef]
7. Mroweh, N.; Pop, F.; Mézière, C.; Allain, M.; Auban-Senzier, P.; Vanthuyne, N.; Alemany, P.; Canadell, E.; Avarvari, N. Combining Chirality and Hydrogen Bonding in Methylated Ethylenedithio-Tetrathiafulvalene Primary Diamide Precursors and Radical Cation Salts. *Cryst. Growth Des.* **2020**, *20*, 2516–2526. [CrossRef]
8. Sahadevan, S.A.; Monni, N.; Abhervé, A.; Auban-Senzier, P.; Canadell, E.; Mercuri, M.L.; Avarvari, N. Synthesis and Physical Properties of Purely Organic BEDT-TTF-Based Conductors Containing Hetero-/Homosubstituted Cl/CN-Anilate Derivatives. *Inorg. Chem.* **2017**, *56*, 12564–12571. [CrossRef]

9. Lopes, G.; Gama, V.; Belo, D.; Simão, D.; Santos, I.C.; Almeida, M.; Rabaça, S. Cyanobenzene–Ethylenedithio–Tetrathiafulvalene Salts with ClO4–: Bilayer Polymorphs and Different Stoichiometries. *Cryst. Growth Des.* **2017**, *17*, 2801–2808. [CrossRef]
10. Baudron, S.A.; Batail, P.; Coulon, C.; Clérac, R.; Canadell, E.; Laukhin, V.; Melzi, R.; Wzietek, P.; Jérome, D.; Auban-Senzier, P.; et al. (EDT-TTF-$CONH_2$)6[Re6Se8(CN)6], a Metallic Kagome-Type Organic−Inorganic Hybrid Compound: Electronic Instability, Molecular Motion, and Charge Localization. *J. Am. Chem. Soc.* **2005**, *127*, 11785–11797. [CrossRef]
11. Rabaça, S.; Oliveira, S.; Santos, I.C.; Gama, V.; Belo, D.; Lopes, E.B.; Canadell, E.; Almeida, M. Polymorphism and Superconductivity in Bilayer Molecular Metals (CNB-EDT-TTF)4I3. *Inorg. Chem.* **2016**, *55*, 10343–10350. [CrossRef] [PubMed]
12. Baudron, S.A.; Avarvari, N.; Batail, P.; Coulon, C.; Clérac, R.; Canadell, E.; Auban-Senzier, P. Singular Crystalline β′-Layered Topologies Directed by Ribbons of Self-Complementary Amide···Amide Ring Motifs in [EDT-TTF-$(CONH_2)_2]_2X$ (X = HSO_4^-, ClO_4^-, ReO_4^-, AsF_6^-): Coupled Activation of Ribbon Curvature, Electron Interactions, and Magnetic Susceptibility. *J. Am. Chem. Soc.* **2003**, *125*, 11583–11590. [CrossRef] [PubMed]
13. Lieffrig, J.; Le Pennec, R.; Jeannin, O.; Auban-Senzier, P.; Fourmigué, M. Toward chiral conductors: Combining halogen bonding ability and chirality within a single tetrathiafulvalene molecule. *CrystEngComm* **2013**, *15*, 4408–4412. [CrossRef]
14. Shin, K.S.; Brezgunova, M.; Jeannin, O.; Roisnel, T.; Camerel, F.; Auban-Senzier, P.; Fourmigué, M. Strong Iodine···Oxygen Interactions in Molecular Conductors Incorporating Sulfonate Anions. *Cryst. Growth Des.* **2011**, *11*, 5337–5345. [CrossRef]
15. Nakano, Y.; Takahashi, Y.; Ishida, K.; Ishikawa, M.; Yamochi, H.; Uruichi, M. Crystal structure and physical properties of radical cation salt based on 4,5-ethylenedioxy-4′-iodotetrathiafulvalene (EDO-TTF-I) with iodine bonding ability. *Mater. Chem. Front.* **2018**, *2*, 752–759. [CrossRef]
16. Shin, K.-S.; Jeannin, O.; Brezgunova, M.; Dahaoui, S.; Aubert, E.; Espinosa, E.; Auban-Senzier, P.; Świetlik, R.; Frąckowiak, A.; Fourmigué, M. Inter-layer charge disproportionation in the dual-layer organic metal (tTTF-I)2ClO4with unsymmetrical I···O halogen bond interactions. *Dalton Trans.* **2014**, *43*, 5280–5291. [CrossRef]
17. Steiner, T. The hydrogen bond in solid state. *Angew. Chem. Int. Ed.* **2002**, *41*, 48–76. [CrossRef]
18. Kanetou, T.; Tsunashima, R.; Hoshino, N.; Akutagawa, T. Solid-state structure and electronic states of hydrogen-bonded dimer of pyridyl-substituted tetrathiafulvalene salted with PF 6? *RSC Adv.* **2017**, *7*, 6236–6241. [CrossRef]
19. Lee, S.C.; Ueda, A.; Kamo, H.; Takahashi, K.; Uruichi, M.; Yamamoto, K.; Yakushi, K.; Nakao, A.; Kumai, R.; Kobayashi, K.; et al. Charge-order driven proton arrangement in a hydrogen-bonded charge-transfer complex based on a pyridyl-substituted TTF derivative. *Chem. Commun.* **2012**, *48*, 8673–8675. [CrossRef]
20. Liu, S.-X.; Dolder, S.; Franz, P.; Neels, A.; Stoeckli-Evans, H.; Decurtins, S. Structural studies of transition metal complexes with 4,5-*Bis*(2-pyridylmethylsulfanyl)-4′,5′-ethylenedithiotetrathiafulvalene: Probing their potential for the construction of multifunctional molecular assemblies. *Inorg. Chem.* **2003**, *42*, 4801–4803. [CrossRef]
21. Jia, C.; Liu, S.-X.; Ambrus, C.; Neels, A.; Labat, G.; Decurtins, S. One-Dimensional μ-Chloromanganese(II)−Tetrathiafulvalene (TTF) Coordination Compound. *Inorg. Chem.* **2006**, *45*, 3152–3154. [CrossRef] [PubMed]
22. Mitamura, Y.; Yorimitsu, H.; Oshima, K.; Osuka, A. Straightforward access to aryl-substituted tetrathiafulvalenes by palladium-catalysed direct C–H arylation and their photophysical and electrochemical properties. *Chem. Sci.* **2011**, *2*, 2017–2021. [CrossRef]
23. Han, Y.-F.; Zhang, J.-S.; Lin, Y.-J.; Dai, J.; Jin, G.-X. Synthesis and characterization of half-sandwich iridium complexes containing 2,6(7)-bis(4-pyridyl)-1,4,5,8-tetrathiafulvalene and ancillary ortho-carborane-1,2-dichalcogenolato ligands. *J. Organomet. Chem.* **2007**, *692*, 4545–4550. [CrossRef]
24. Wang, R.; Kang, L.-C.; Xiong, J.; Dou, X.; Chen, X.-Y.; Zuo, J.-L.; You, X.-Z. Structures and physical properties of oligomeric and polymeric metal complexes based on bis(pyridyl)-substituted TTF ligands and an inorganic analogue. *Dalton Trans.* **2011**, *40*, 919–926. [CrossRef] [PubMed]

25. Tang, Z.-Z.; Weng, Y.-G.; Yin, W.-Y.; Jiang, M.; Zhu, Q.-Y.; Dai, J. A Potential Hybrid Hole-Transport Material Incorporating a Redox-Active Tetrathiafulvalene Derivative with CuSCN. *Inorg. Chem.* **2019**, *58*, 15824–15831. [CrossRef] [PubMed]
26. Yin, Z.-N.; Li, Y.-H.; Sun, Y.-G.; Chen, T.; Xu, J.; Zhu, Q.-Y.; Dai, J. 3D Copper Tetrathiafulvalene Redox-Active Network with 8-Fold Interpenetrating Diamond-like Topology. *Inorg. Chem.* **2016**, *55*, 9154–9157. [CrossRef] [PubMed]
27. Zappe, L.; Schönfeld, S.; Hoerner, G.; Zenere, K.A.; Leong, C.F.; Kepert, C.J.; D'Alessandro, D.M.; Weber, B.; Neville, S.M. Spin crossover modulation in a coordination polymer with the redox-active bis-pyridyltetrathiafulvalene (py2TTF) ligand. *Chem. Commun.* **2020**, *56*, 10469–10472. [CrossRef]
28. Sherman, D.A.; Murase, R.; Duyker, S.G.; Gu, Q.; Lewis, W.; Lu, T.; Liu, Y.; D'Alessandro, D.M. Reversible single crystal-to-single crystal double [2+2] cycloaddition induces multifunctional photo-mechano-electrochemical properties in framework materials. *Nat. Commun.* **2020**, *11*, 1–10. [CrossRef]
29. Cerrada, E.; Laguna, M.; Bartolomé, J.; Campo, J.; Orera, V.; Jones, P.G. Cation-radical salts with organometallic gold anions. X-ray structure of [TTFPh]2[Au(C6F5)2]. *Synth. Met.* **1998**, *92*, 245–251. [CrossRef]
30. Sheldrick, G. SHELXT– Integrated space-group and crystal-structure determination. *Acta Crystallogr. Sect. A Found. Adv.* **2015**, *71*, 3–8. [CrossRef]
31. Sheldrick, G.M. Crystal structure refinement with SHELXL. *Acta Crystallogr. Sect. C Struct. Chem.* **2015**, *C71*, 3–8. [CrossRef] [PubMed]
32. Dolomanov, O.V.; Bourhis, L.J.; Gildea, R.J.; Howard, J.A.K.; Puschmann, H. OLEX2: A complete structure solution, refinement and analysis program. *J. Appl. Cryst.* **2009**, *42*, 339–341. [CrossRef]
33. *Gaussian 16, Revision C.01*; Gaussian, Inc.: Wallingford, CT, USA, 2016.
34. Boys, S.; Bernardi, F. The calculation of small molecular interactions by the differences of separate total energies. Some procedures with reduced errors. *Mol. Phys.* **1970**, *19*, 553–566. [CrossRef]
35. Becke, A.D. A new mixing of Hartree–Fock and local density—Functional theories. *J. Chem. Phys.* **1993**, *98*, 1372–1377. [CrossRef]
36. Lee, C.; Yang, W.; Parr, R.G. Development of the Colle-Salvetti correlation-energy formula into a functional of the electron density. *Phys. Rev. B* **1988**, *37*, 785–789. [CrossRef]
37. Miehlich, B.; Savin, A.; Stoll, H.; Preuss, H. Results obtained with the correlation energy density functionals of becke and Lee, Yang and Parr. *Chem. Phys. Lett.* **1989**, *157*, 200–206. [CrossRef]
38. Kendall, R.A.; Dunning, T.H., Jr. Electron affinities of the first–row atoms revisited. Systematic basis sets and wave functions. *J. Chem. Phys.* **1992**, *96*, 6796–6806. [CrossRef]
39. Del Bene, J.E.; Person, W.B.; Szczepaniak, K. Properties of Hydrogen-Bonded Complexes Obtained from the B3LYP Functional with 6-31G(d,p) and 6-31+G(d,p) Basis Sets: Comparison with MP2/6-31+G(d,p) Results and Experimental Data. *J. Phys. Chem.* **1995**, *99*, 10705–10707. [CrossRef]
40. Shultz, M.J.; Vu, T.H. Hydrogen Bonding between Water and Tetrahydrofuran Relevant to Clathrate Formation. *J. Phys. Chem. B* **2015**, *119*, 9167–9172. [CrossRef]
41. Joshi, R.; Ghanty, T.K. Hydrogen bonding interaction between HO2 radical and selected organic acids, RCOOH (R=CH3, H, Cl and F). *Chem. Phys. Lett.* **2013**, *584*, 43–48. [CrossRef]
42. Gao, H.; Zhang, Y.; Wang, H.-J.; Liu, J.; Chen, J. Theoretical Study on the Structure and Cation–Anion Interaction of Amino Acid Cation Based Amino Acid Ionic Liquid [Pro]+[NO3]$^{-}$. *J. Phys. Chem. A* **2010**, *114*, 10243–10252. [CrossRef] [PubMed]
43. Velde, G.; Bickelhaupt, F.M.; Baerends, E.J.; Guerra, C.F.; van Gisbergen, S.J.A.; Snijders, J.G.; Ziegler, T. Chemistry with ADF. *J. Comput. Chem.* **2001**, *22*, 931–967. [CrossRef]
44. *ADF 2019.3, SCM, Theoretical Chemistry*; Vrije Universiteit: Amsterdam, The Netherlands. Available online: https://www.scm.com/product/adf/ (accessed on 26 November 2020).
45. *AMS DFTB 2019.3, SCM, Theoretical Chemistry*; Vrije Universiteit: Amsterdam, The Netherlands. Available online: https://www.scm.com/product/ams/ (accessed on 26 November 2020).
46. Levi, O.P.-T.; Becker, J.Y.; Ellern, A.; Khodorkovsky, V. Synthesis of 2,3-dimethylthio-6-pyridyl tetrathiafulvalene: A precursor for a new system involving a direct linkage between a strong donor (D) and a strong acceptor (A). *Tetrahedron Lett.* **2001**, *42*, 1571–1573. [CrossRef]

47. Crystallographic data for TTF-py2_PF6: C52H42F12N6O2P2S12, M = 1457.57, T = 120 K, Monoclinic, Space group P21/c, Z = 2, a = 10.5747(10) Å, b = 13.6826(7) Å, c = 19.9351(11) Å, β = 90.256(6)°, V = 2884.4(3) Å3, Dc = 1.678 mg cm–3, 16917 reflections collected, final R1 and wR2 (I > 2σ(I)) = 0.0910 and 0.2264. CCDC deposition number 2040487. Available online: https://www.ccdc.cam.ac.uk/ (accessed on 26 November 2020).
48. Bondi, A. van der Waals Volumes and Radii. *J. Phys. Chem.* **1964**, *68*, 441–451. [CrossRef]
49. Matsuzaki, S.; Moriyama, T.; Toyoda, K. Raman spectra of mixed valent TTF salts; relation between Raman frequency and formal charge. *Solid State Commun.* **1980**, *34*, 857–859. [CrossRef]
50. Rosokha, S.V.; Kochi, J.K. Molecular and Electronic Structures of the Long-Bonded π-Dimers of Tetrathiafulvalene Cation-Radical in Intermolecular Electron Transfer and in (Solid-State) Conductivity. *J. Am. Chem. Soc.* **2007**, *129*, 828–838. [CrossRef]
51. Scott, B.A.; La Placa, S.J.; Torrance, J.B.; Silverman, B.D.; Welber, B. The crystal chemistry of organic metals. Composition, structure, and stability in the tetrathiafulvalinium-halide systems. *J. Am. Chem. Soc.* **1977**, *99*, 6631–6639. [CrossRef]
52. Torrance, J.B.; Scott, B.A.; Welber, B.; Kaufman, F.B.; Seiden, P.E. Optical properties of the radical cation tetrathiafulvalenium (TT F+) in its mixed-valence and monovalence halide salts. *Phys. Rev. B* **1979**, *19*, 730–741. [CrossRef]
53. Jacobsen, C.S. *Optical Properties in Semiconductors and Semimetals*; Conwell, E., Ed.; Academic Press: Boston, MA, USA, 1988; Volume 27, pp. 293–384.
54. Kittel, C. *Introduction to Solid State Physics*; Wiley: Hoboken, NJ, USA, 2004.
55. Wood, P.A.; Allen, F.H.; Pidcock, E. Hydrogen-bond directionality at the donor H atom—Analysis of interaction energies and database statistics. *CrystEngComm* **2009**, *11*, 1563–1571. [CrossRef]
56. Qu, L.; Iguchi, H.; Takaishi, S.; Habib, F.; Leong, C.F.; D'Alessandro, D.M.; Yoshida, T.; Abe, H.; Nishibori, E.; Yamashita, M. Porous Molecular Conductor: Electrochemical Fabrication of Through-Space Conduction Pathways among Linear Coordination Polymers. *J. Am. Chem. Soc.* **2019**, *141*, 6802–6806. [CrossRef] [PubMed]
57. Koyama, S.; Tanabe, T.; Takaishi, S.; Yamashita, M.; Iguchi, H. Preliminary chemical reduction for synthesizing a stable porous molecular conductor with neutral metal nodes. *Chem. Commun.* **2020**, *56*, 13109–13112. [CrossRef] [PubMed]
58. Koo, J.Y.; Yakiyama, Y.; Lee, G.R.; Lee, J.; Choi, H.C.; Morita, Y.; Kawano, M. Selective Formation of Conductive Network by Radical-Induced Oxidation. *J. Am. Chem. Soc.* **2016**, *138*, 1776–1779. [CrossRef] [PubMed]
59. Chen, D.; Xing, H.; Su, Z.-M.; Wang, C. Electrical conductivity and electroluminescence of a new anthracene-based metal–organic framework with π-conjugated zigzag chains. *Chem. Commun.* **2016**, *52*, 2019–2022. [CrossRef] [PubMed]
60. Park, S.S.; Hontz, E.R.; Sun, L.; Hendon, C.H.; Walsh, A.; Van Voorhis, T.; Dincă, M. Cation-Dependent Intrinsic Electrical Conductivity in Isostructural Tetrathiafulvalene-Based Microporous Metal–Organic Frameworks. *J. Am. Chem. Soc.* **2015**, *137*, 1774–1777. [CrossRef] [PubMed]
61. Skorupskii, G.; Trump, B.A.; Kasel, T.W.; Brown, C.M.; Hendon, C.H.; Dincă, M. Efficient and tunable one-dimensional charge transport in layered lanthanide metal-organic framworks. *Nat. Chem.* **2020**, *12*, 131–136. [CrossRef]